Seasonal Predictability of Bottom Temperatures along the North American West Coast

Tongtong Xu[1,2], Matthew Newman[1], Michael A. Alexander[1], and Antonietta Capotondi[1,2]

[1] NOAA Physical Sciences Laboratory, Boulder, CO.

[2] CIRES, University of Colorado, Boulder, CO.

Corresponding author: Tongtong Xu (tongtong.xu@noaa.gov)

Key Points:

- Bottom Temperature (BT) forecasts along the North American West Coast by a Linear Inverse Model (LIM) are more skillful than persistence.
- Elevated BT forecast skill is linked to ENSO, with a delayed response along the coast relative to the tropical Pacific.
- BT predictability is higher at locations with ~50-150m bathymetric depth, and in Canadian waters.

Abstract

Bottom Temperature (BT) along the North American West Coast strongly influences benthic and demersal marine species. However, since high-resolution coastal-wide data and prediction systems are lacking, seasonal BT forecast efforts have been limited and sources of BT predictability largely undiagnosed. Here, an empirical model called a Linear Inverse Model (LIM), constructed from a high-resolution ocean reanalysis, is used to predict BTs along the North American West Coast and to identify "forecasts of opportunity" when BTs may be especially predictable. The LIM is considerably more skillful than persistence, particularly when targeting winter, with anomaly correlation skill values of 0.6 at six month lead. As identified a priori through analysis of the LIM's dynamics, elevated forecast skill is linked to El Niño-Southern Oscillation (ENSO), which drives a predicted BT response whose peak occurs later with increasing latitude. We find that ENSO therefore drives the BT forecasts of opportunity, with skill of hindcasts corresponding to the top quintile of ENSO events reaching 0.6 at six month lead, while the remaining 80% of the hindcasts has skill of only 0.4. Also, forecast skill is maximized for locations where bathymetry depths are around 50-150m, which is anticipated from the LIM's forecast signal-to-noise ratio.

Plain Language Summary

Ocean bottom conditions, such as Bottom Temperatures (BT), can directly affect the ecosystem of the benthic and demersal marine species along the North American West Coast. Due to the lack of high-resolution data and prediction systems, seasonal forecasts of BT and diagnosis of BT predictability have been limited. In this study, we construct a multivariate linear dynamical model, called a Linear Inverse Model (LIM), to predict BTs along the North American West

Coast and to identify the circumstances and timing when BTs may be especially predictable. We find the LIM predictions are substantially more skillful than the baseline, i.e., simply taking the current ocean anomalies as the future predicted states, a simplest approach possible. Furthermore, the LIM prediction skill is mainly improved when targeting winter, which is linked to El Niño-Southern Oscillation (ENSO), the dominant phenomenon of interannual variability of the climate system. The LIM prediction skill is maximized for locations where bathymetry depths are around 50-150m, which may be related to different processes influencing ocean characteristics of different depths.

1 Introduction

The coastal ocean along the North American West Coast is an essential ecosystem habitat, which naturally supplies numerous nutrients critical for the living of marine species, and in turn contributes to high proportion of commercial fish yield (e.g., Capone & Hutchins 2013; Stock et al. 2015). Among relevant physical drivers, ocean temperature has been identified as a leading factor affecting the physiological processes of aquatic organisms and species (e.g., Drinkwater et al. 2010; Ottersen et al. 2010; Sampaio & Rosa 2020). Thus, skillful forecasts of ocean temperature are key to reliably predict future ecosystem fluctuations and provide guidance on mitigation strategies.

Predictions of ocean temperatures have mainly focused at the surface, which is more easily measured and observed than the deeper ocean. Sea Surface Temperature (SST) seasonal forecasts along the North American West Coast have shown skill (e.g., Stock et al. 2015; Hervieux et al. 2019; Jacox et al. 2019), apparently associated with local and remote effects of El

Niño-Southern Oscillation (ENSO) (e.g., Wen et al. 2012; Capotondi et al. 2019a; Jacox et al. 2019). During ENSO development, equatorial Kelvin waves propagate eastward along the equator, and then continue poleward along the coast as coastally-trapped Kelvin waves, inducing thermocline variability (e.g., Jacox et al. 2015; Engida et al. 2016; Ray et al. 2020; Amaya et al. 2022). These coastally-trapped waves have amplitude and offshore scale that decrease with latitude (e.g., Hermann et al. 2009; Frischknecht et al. 2015; Gómez-Valdivia et al. 2017), so that they may be more impactful in the lower-latitude coastal waters. At higher latitudes, changes in atmospheric circulation associated with ENSO atmospheric teleconnections may play a greater role. These atmospheric circulation changes involve a deepening and eastward displacement of the Aleutian Low, causing variations in the alongshore winds and coastal upwelling (e.g., Hermann et al. 2009; Jacox et al. 2015; Ding et al. 2021), and usually follow the ENSO peak phase by a few months (e.g., Deser & Blackmon 1995; Alexander et al. 2002; Liu & Alexander 2007).

On the other hand, ocean bottom conditions can directly affect the abundance and distribution of benthic and demersal marine species (e.g., Keller et al. 2015; Barbeaux et al. 2020; Norton et al. 2020), so forecasting Bottom Temperatures (BT), or ocean temperatures along the continental shelf, is also very important. Recent studies (Alexander et al. 2023; Amaya et al. 2023) have shown that BTs are highly correlated with SSTs in relatively shallow regions, where the mixed layer can extend close to the sea floor, suggesting that in those regions, mechanisms contributing to SST variability and predictability may also contribute to the predictability of BT. In addition to mixed layer dynamics, vertical movements of the thermocline, due, e.g., to coastal wave propagation or variability of coastal upwelling, can also influence both SSTs and BTs in those regions where the ocean depth is similar to thermocline depth. Deep locations below the thermocline, on the other hand, may experience variability that is unrelated to SST, but more affected by subsurface ocean currents (e.g., the California undercurrent) and their interactions with the local bathymetry (e.g., Breaker 2019; Kurczyn et al. 2019; Ray et al. 2020).

Until now, only a few studies have examined BT forecasts and the sources of BT predictability. The main tools for seasonal predictions are climate models. Yet the resolution of the current generation of climate models is relatively coarse, and unable to sufficiently capture the shelf-scale dynamics and coastal processes (Stock et al. 2011). This has led to efforts using dynamical downscaling techniques (see reviews by Jacox et al. 2020), which typically involve the use of a regional ocean model forced at the ocean surface and lateral boundaries by the output of a global model. Studies that used dynamical downscaling to predict BT showed differences in skill in different regions. For example, the dynamical downscaling conducted by JISAO's Seasonal Coastal Ocean Prediction of the Ecosystem (J-SCOPE) (Siedlecki et al. 2016), for Washington and Oregon coastal waters, indicated that BTs are more realistically simulated than SSTs and that BT forecasts are more skillful at mid-shelf locations than at shallower sites. On the other hand, another dynamical downscaling application in the Eastern Bering Sea Shelf (Kearney et al. 2021), a region strongly affected by seasonal sea ice cover, suggested that the BT forecast skill is only marginally better than persistence, and that sea ice is a prediction barrier. For the California Current System, dynamical downscaled forecasts exhibit greater persistence and better forecasts of BT than SST; the skill of both is mainly associated with ENSO teleconnections (Jacox et al. in review). These examples demonstrate the potential of dynamical downscaling in delivering useful BT forecasts.

However, these dynamical downscaling approaches can be computationally very expensive, an aspect that poses significant limitations to the feasibility of probabilistic forecasts where several ensemble members are needed. In addition, the results obtained with the regional systems may be strongly impacted by the potential biases of the global models that provide the surface forcing and lateral boundary conditions for those systems, possibly introducing errors in the predicted fields (Capotondi et al. 2019b; Jacox et al. 2020). These issues with dynamical downscaling make alternative statistical approaches very attractive. For example, a set of simple linear regression models using indices (such as Gulf Stream indices) to predict BT along the Northeast U.S. Continental Shelf found that oceanic advection, from both the north (Labrador Current) and from the south (Gulf Stream), contributes to enhance BT hindcast skill beyond the persistence (Chen et al. 2021). These results were made possible by the recent release of GLORYS12v1 ocean reanalysis (Lellouche et al. 2021), an eddy-resolving global ocean product with sufficient horizontal resolution (1/12º, ~9km) to reasonably resolve the North American coastal environment (Alexander et al. 2023; Amaya et al. 2023). These results suggest the potential of other applications of this reanalysis for BT forecasts using statistical approaches.

A multivariate empirical dynamical approach that has proven useful in climate prediction is the Linear Inverse Model (LIM; Penland & Sardeshmukh 1995). Numerous studies have shown that LIMs realistically capture the seasonal evolution of surface anomalies in the Pacific sector (e.g., Alexander et al. 2008; Lou et al. 2020; Xu et al. 2021; Zhao et al. 2021; Capotondi et al. 2022), making SST forecasts with skill comparable to operational forecast models (e.g., Newman & Sardeshmukh 2017; Shin & Newman 2021). Additionally, the LIM can estimate potential predictability, of both itself and other forecast models (e.g., Newman & Sardeshmukh

2017), including determining -- in advance -- forecasts with potentially higher prediction skill, sometimes called "forecasts of opportunity" (e.g., Albers & Newman 2019; Mariotti et al. 2020).

Motivated by these studies, we construct a LIM for the Pacific basin, to forecast BTs along the North American West Coast on seasonal timescales. By applying the LIM to BTs, we aim to answer the following questions: (a) how well can we forecast BTs in this region, and (b) can we identify key mechanisms or conditions conducive to skillful BT forecasts? The paper is organized as follows. In Section 2, we describe the ocean reanalysis state variables and their preprocessing, followed by an introduction of the LIM methodology and its application to the identification of "forecasts of opportunity", within the LIM framework. In Section 3, we present our hindcast results, including the seasonal and bathymetric depth dependence of the hindcast skill, and highlight how the BT predictability is linked to ENSO. A summary is described in Section 4.

2 Data and Methods

2.1 Data

We use monthly BTs, SSTs, and Sea Surface Heights (SSHs) over the years 1993-2019 from the GLORYS12v1 ocean reanalysis (Lellouche et al. 2021), chosen for its reasonably good representation of the North American coastal environment (e.g., see Alexander et al. 2023; Amaya et al. 2023; and references therein). We focus on BT along the North American West Coast, spanning 15°-60°N, 145°-100°W, and for bottom depths to 400 m (Fig. 1). Pacific basin SST and SSH (extending from 20°S-60°N and from 100°E-68°W) are incorporated for their potential contribution to BT forecasts. Anomalies of each field (BTA, SSTA, SSHA) are obtained by removing the seasonal mean climatology and subtracting the linear trend. While the long-term trend has evolved nonlinearly within some regions (Frankignoul et al. 2017; Xu et al. 2022), a linear estimate may be reasonable for the short period of 1993-2019.

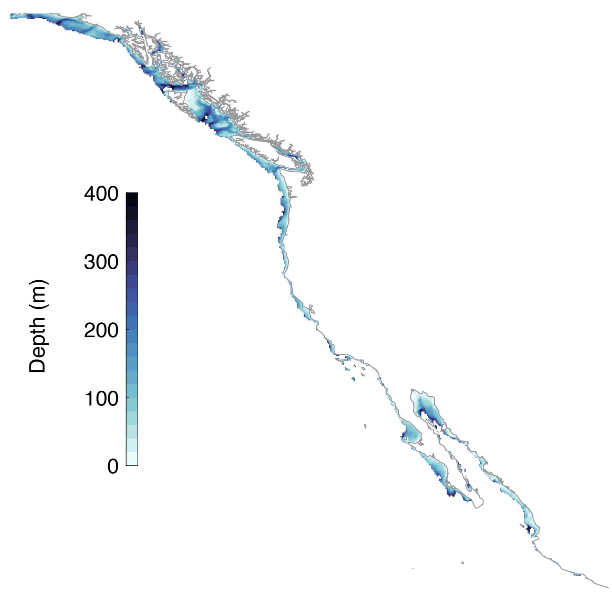

Figure 1. Bathymetry depth (m) along the North American West Coast.

2.2 Linear Inverse Model

A LIM assumes that the evolution of coarse-grained climate anomalies can be approximated by deterministic linear dynamics plus unpredictable (rapidly decorrelating) nonlinearities represented as stochastic white noise forcing, or:

$$\frac{\mathrm{d}\mathbf{x}}{\mathrm{d}t} = \mathbf{Lx} + \boldsymbol{\xi} \qquad (1)$$

where $\mathbf{x}(t)$ is a climate anomaly state vector, $\mathbf{L}$ is a stable linear dynamical operator, $\boldsymbol{\xi}(t)$ is temporally white noise (which can have spatial coherence determined from a balance relation), and t is time (Penland & Sardeshmukh 1995). $\mathbf{L}$ is determined from the observed simultaneous and lagged covariances of $\mathbf{x}(t)$, as described in Penland & Sardeshmukh (1995) and Newman et al. (2003):

$$\mathbf{L} = \tau_0^{-1} \ln(\mathbf{C}(\tau_0)\mathbf{C}(0)^{-1}) \tag{2}$$

in which $\mathbf{C}(0) = \langle \mathbf{x}(t)\mathbf{x}(t)^{\mathrm{T}} \rangle$ is the auto-covariance matrix, $\mathbf{C}(\tau_0) = \langle \mathbf{x}(t+\tau_0)\mathbf{x}(t)^{\mathrm{T}} \rangle$ is the lag-τ_0 covariance, and τ_0 denotes the time lag between $\mathbf{x}(t)$ and $\mathbf{x}(t+\tau_0)$. Note that τ_0 is a training lag. If (1) is a reasonable representation of the climate dynamical evolution, the resulting L operator should be independent of the chosen τ_0, and capable of accurately reproducing lag-covariance statistics at lags longer than the training lag (Penland & Sardeshmukh 1995). Here we chose $\tau_0 = 1$ month, following previous studies that have tested the suitability of such a training lag (e.g., Newman & Sardeshmukh 2017; Shin & Newman 2021; Xu et al. 2022).

Having obtained $\mathbf{L}$, ensemble-mean forecasts for any lead time τ are

$$\hat{\mathbf{x}}(t+\tau) = \exp(\mathbf{L}\tau)\,\mathbf{x}(t) \equiv \mathbf{G}(\tau)\mathbf{x}(t), \tag{3}$$

with expected forecast error variance determined by the diagonal of

$$\mathbf{E}(\tau) = \mathbf{C}(0) - \mathbf{G}(\tau)\mathbf{C}(0)\mathbf{G}(\tau)^{\mathrm{T}} \tag{4}$$

in which $\mathbf{E}(\tau)$ is the expected forecast error covariance matrix, and $\mathbf{G}(\tau) \equiv \exp(\mathbf{L}\tau)$ is the Green's function.

In our study, $\mathbf{x}(t)$ consists of coastal BTA, Pacific SSTA and SSHA. To reduce dimensionality, anomalies of each field were first projected on their Empirical Orthogonal Functions (EOFs), and associated time evolving amplitudes, i.e., Principal Components (PCs). $\mathbf{x}(t)$ is then constructed by a leading subset of PCs of each field. We retain the leading 15/9/8 PCs of BTA/SSTA/SSHA, representing 84/54/39% of each field's variance. This combination of

PCs is chosen to maximize the cross-validated forecast skill of BTA. Truncating to different numbers of PCs does not fundamentally change our results.

Following previous LIM studies (e.g., Newman & Sardeshmukh 2017; Shin & Newman 2021; Breeden et al. 2022), independent hindcast skill is evaluated through ten-fold cross-validation. This is done by first dividing the data record into 10 subsamples with equivalent lengths. We compute the linear operator **L** from 90% of the data record (i.e., 9 subsamples). This **L** is then applied to the remaining 10% record (i.e., 1 subsample), which serve as initial conditions to obtain the subsequent 1-12 month forecast. This process is repeated ten times to obtain forecasts for each 10% record, which are then concatenated together into the forecast time series over the full length of the data record. Hindcast skill is measured using local anomaly correlation between the hindcasts and their corresponding observed verifications.

2.3 Diagnosing LIM predictability

In some sense, predictability (or potential forecast skill) represents a tradeoff between a deterministic (predictable) signal and the inherent uncertainty induced by unpredictable noise (Lorenz 1963; Scaife & Smith 2018). It therefore may be assessed using a forecast signal-to-noise ratio, which in the LIM is easily determined using (3) and (4) from the ratio of the forecast variance and the expected error variance. The expected LIM forecast skill (e.g., measured by anomaly correlation) is then a monotonic function of this ratio (Sardeshmukh et al. 2000).

Since forecast error variance from (4) depends only on lead time and not on the initial anomaly, case-to-case variations in expected LIM forecast skill are entirely determined by variations of forecast amplitude in (3) (Newman et al. 2003). Forecasts of opportunity may therefore be identified in advance by determining relatively small-amplitude initial conditions that undergo maximum anomaly amplification over some finite time interval τ (e.g., Breeden et al. 2020; Capotondi et al. 2022). Such "optimal precursors" are identified by the amplitude ratio γ^2 between an initial and a final state over the time interval τ, measured by

$$\gamma^2(\tau) = \frac{\mathbf{x}(t)^{\mathrm{T}}\mathbf{G}(\tau)^{\mathrm{T}}\mathbf{N}\mathbf{G}(\tau)\mathbf{x}(t)}{\mathbf{x}(t)^{\mathrm{T}}\mathbf{x}(t)} \tag{5}$$

where **N** is a matrix representing a final pattern or target variable of interest (Farrell 1988). In this study, we use **N** to target BTA throughout the coastal domain, such that

$$\mathbf{N} = \begin{bmatrix} \mathbf{I} & \\ & 0 \end{bmatrix} \tag{6}$$

where **I** is the identity matrix, i.e., only diagonal elements corresponding to BTA are 1 and all other elements are 0. This **N** is to maximize the ratio between the amplitude of the evolved BTA and the amplitude of the initial conditions, with the aim of identifying precursors leading to particularly skillful BTA predictions. The optimal precursor that subsequently leads to maximum BTA growth over a given time interval τ is simply the leading eigenvector of $\mathbf{G}(\tau)^{\mathrm{T}}\mathbf{N}\mathbf{G}(\tau)$.

3 Results

3.1 North American West Coast BTA Variability

Along the West Coast, BTA variability is dominated by a pattern with larger magnitude in the southern (Baja California) than in the northern parts of the domain, captured by the leading EOF of BTA (Fig. 2a). The dominant patterns of Pacific SSTA and SSHA (EOFs shown in Fig. 2b) are both typical of the mature phase of ENSO: large SSTA amplitude in the central and eastern Pacific, and an east-west SSH dipole indicative of a deeper (shallower) thermocline in the eastern Pacific and a shallower (deeper) thermocline in the western Pacific (e.g., Meinen & McPhaden 2000; Capotondi et al. 2020). The time evolving amplitudes of the leading EOFs for each field (i.e., their PCs), are shown in Fig. 2c. While each field's dominant pattern is determined separately, their PCs are highly correlated ($r = 0.8$), suggesting that BTA along the North American West Coast may be linked to ENSO variability in the tropical Pacific.

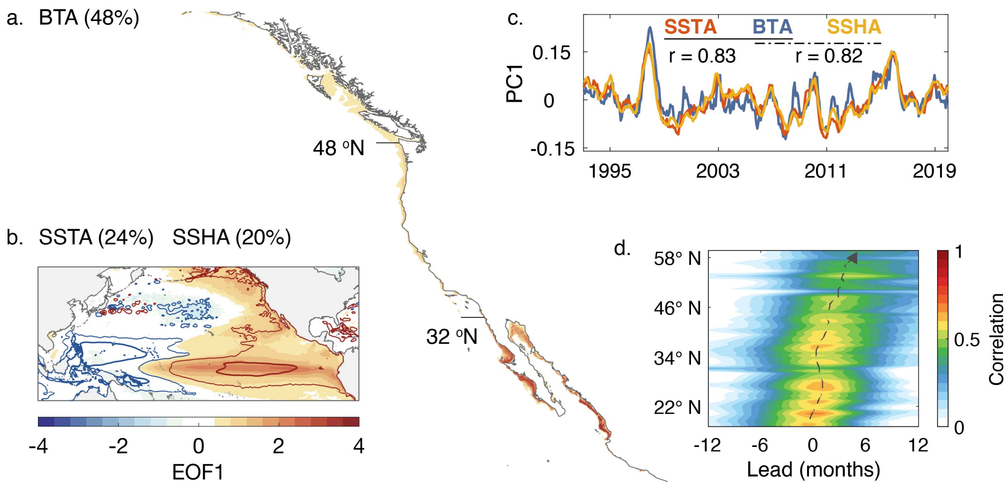

Figure 2. Dominant patterns of variability. The leading Empirical Orthogonal Function (EOF1) of (a) Bottom Temperature Anomaly (BTA), (b) Sea Surface Temperature Anomaly (SSTA; shading), and Sea Surface Height Anomaly (SSHA; contour). Contour is SSHA at values 2 (thin), 4 (thick) (positive: red; negative: blue). Percentage variance explained by each EOF1 is marked. (c) The corresponding Principal Component (PC1) of BTA (blue), SSTA (red), and SSHA (orange). Correlations between PC1 of different variables are indicated on top of panel c. EOF1/PC1 of each field is separately normalized for display purpose. (d) Lead-lag correlation (x-axis) between SSTA PC1 and local BTA, derived for each grid point, averaged for every 0.6° latitudinal bin, and displayed as a function of latitude (y-axis). Positive (negative) leads denote SSTA PC1 preceding (following) local BTA. Dashed line is the peak correlation at each latitude.

As ENSO may exhibit its influence along the coast with different lags, we may expect some lead-lag response between ENSO and BTA variability. Indeed, we find ENSO tends to lead BTA along the West Coast by a few months, illustrated by the lead-lag correlation between the leading SSTA PC and the BTA time series determined for each latitude along the coast (Fig. 2d). BTA variations appear quasi-synchronous with ENSO in the southern part of the coastal domain, since BTA is maximally correlated there with the leading SSTA PC at about 0-month lag. Moving poleward, the correlation peaks at gradually longer lags (~5 months in the north), indicating a delayed response of the coastal BTA signal to ENSO. A similar delayed response has been found between SSTA in the California Current System and the tropical Pacific (e.g., Jacox et al. 2019).

3.2 Skillful Seasonal BTA Prediction

The potential link between BTA along the North American West Coast and ENSO motivates the construction of the Pacific LIM (section 2.2) and its use for seasonal BTA prediction. Figure 3 compares the LIM's BTA hindcast skill to persistence, which gauges how much prediction skill is due to local memory alone, often used as a baseline for prediction skill of many ocean variables (e.g., Qiu et al. 2014; Jacox et al. 2019; Amaya et al. 2022). Evaluated in terms of local anomaly correlation, the 6-month-lead persistence skill (Fig. 3a) is ~0.3 on average, and the 12-month-lead persistence skill (Fig. 3b) is only ~0.1.

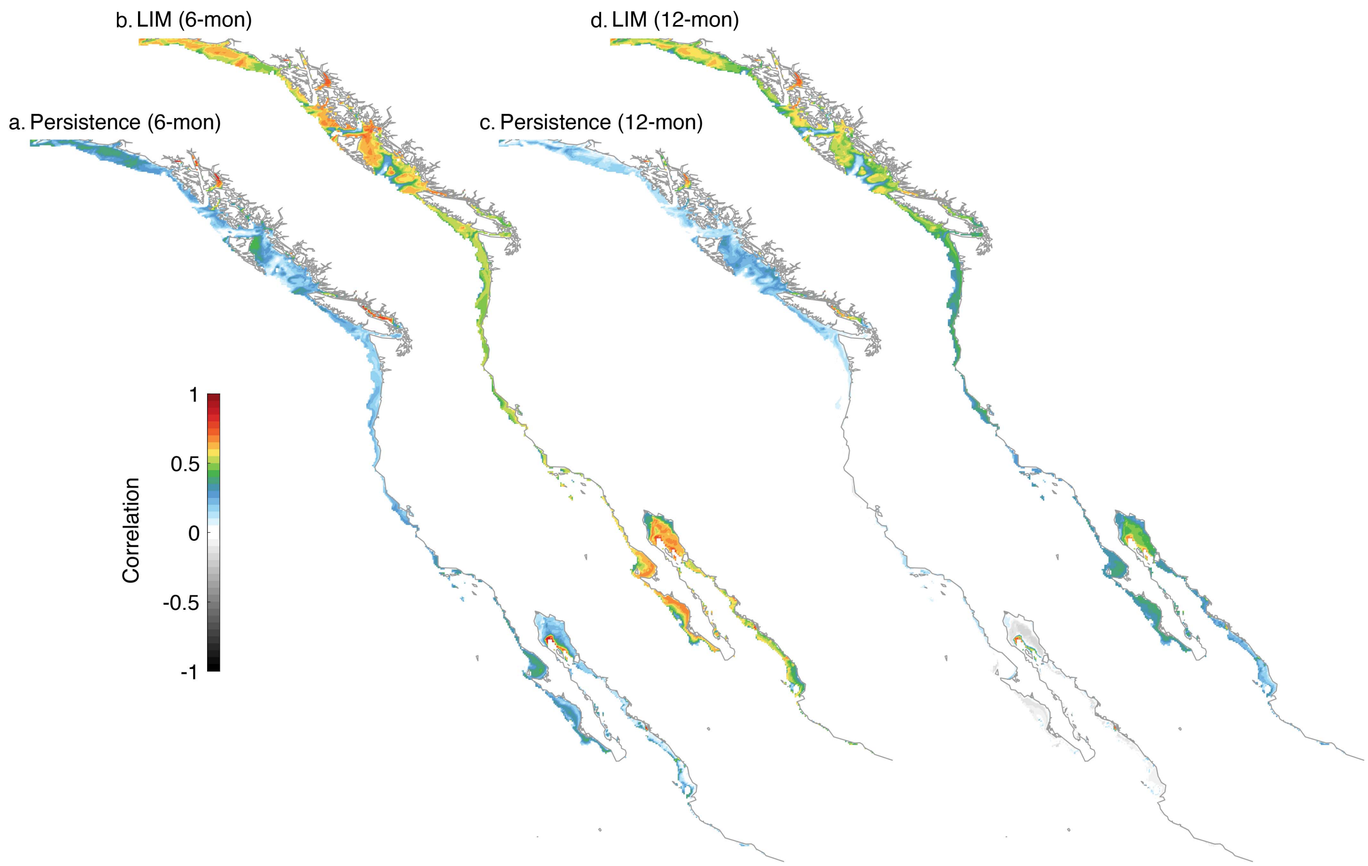

Figure 3. BTA hindcast skill (anomaly correlation) comparison between persistence and Linear Inverse Model (LIM). (a) 6-, (c) 12-month-lead persistence, and (b) 6-, (d) 12-month-lead LIM hindcast skill.

LIM hindcasts are significantly more skillful than persistence in most locations. Skill values are as high as ~0.6 for leads of 6 months in Canadian coastal waters and along Baja California (Fig. 3c), and still ~0.6 at 12-month lead in Canadian waters (Fig. 3d). Skill determined separately for southern, central, and northern sub-regions is shown as a function of verification month and lead time in Fig. 4. For all three sub-regions (Fig. 4a-c), skill values are significant for LIM hindcasts verified during winter/spring, for lead times up to ~10-12 months.

When verifying during summer/fall, LIM hindcast skill is generally lower, especially in the southern and central sub-regions. ENSO seasonality has been found to drive similar seasonal variations in skill for coastal SSTA, SSHA, BTA, and stratification forecasts (Jacox et al. 2019; Shin & Newman 2021; Jacox et al. in review), and it may be similarly influencing LIM BTA hindcast.

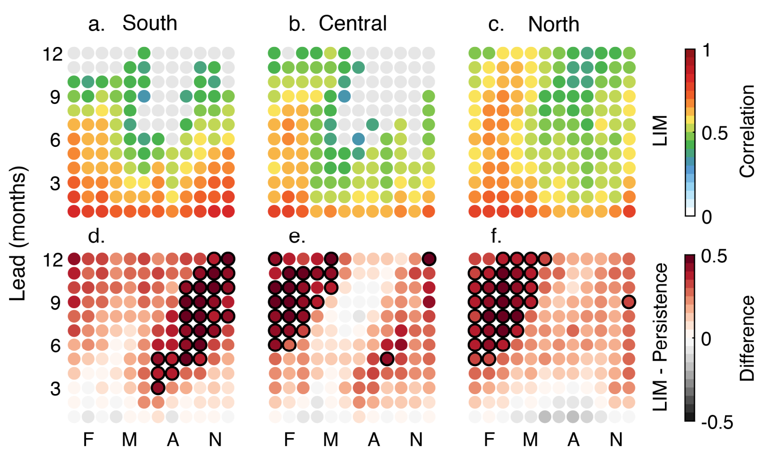

Figure 4. (a-c) LIM forecast skill at 1-12 month leads compared to (d-f) persistence, spatially averaged for (a, d) southern (south of 32ºN), (b, e) central (32ºN~48ºN), and (c, f) northern (north of 48ºN) sub-regions. (a-c) LIM hindcast skill, where color dots represent significant skill values (95% confidence level based on bootstrapping). (d-f) Difference between LIM and persistence skill, where dots with black outlines indicate LIM skill significantly above persistence (95% confidence level). Verification month is on the x-axis, lead time is on the y-axis. See Fig. 2a for the geographic range of each sub-region.

There is also both a seasonal and latitudinal dependence to the locations and times when LIM prediction of BTA is relatively more skillful. In the southern sub-region, the LIM is significantly more skillful than persistence in the late fall and the early winter (Fig. 4d). Moving poleward, the central sub-region shows significantly enhanced skill relative to persistence in late winter (Fig. 4e) and the northern sub-region is improved in early spring (Fig. 4f). This relatively high skill, moving northward from fall to winter to spring, suggests that the LIM dynamics capture the observed northward progression of the ENSO influence seen in Fig. 2d.

3.3 Dependence of BTA Hindcast Skill on Bathymetric Depth

We next evaluate how BTA hindcast skill varies as a function of bathymetry depth and lead time (Fig. 5a-c), obtained by partitioning the range of bathymetric depths into 20m bins, with hindcast skill averaged over each depth bin and lead time. This calculation is repeated separately for each sub-region.

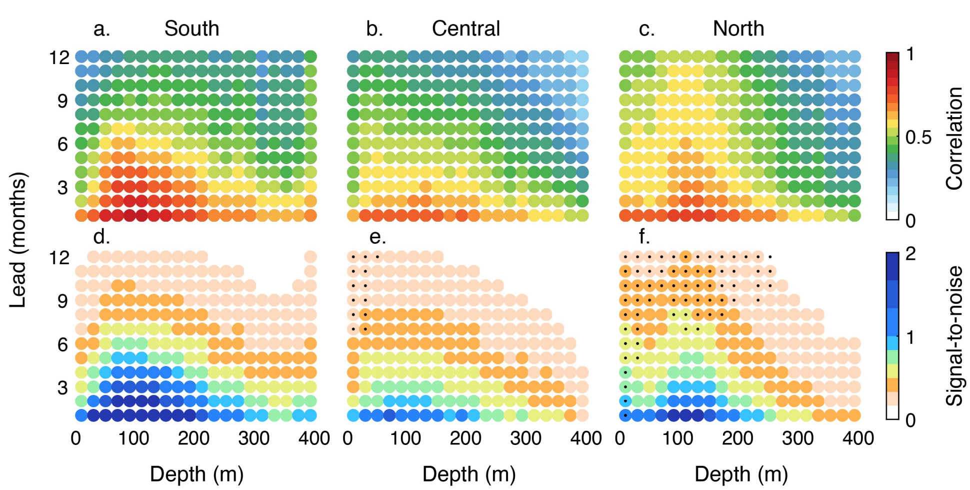

Figure 5. BTA (a-c) hindcast skill (anomaly correlation) and (d-f) signal-to-noise ratio, as a function of bathymetry depth and lead time. Each metric is separately evaluated for (a, d) southern, (b, e) central, and (c, f) northern sub-regions. The bathymetry depth is on the x-axis.

Lead time is shown on the y-axis. (e, f) Black dots denote signal-to-noise ratio at a certain depth and lead time is higher than its counterpart in (d).

Overall, hindcasts tend to be least skillful at locations with either the shallowest or deepest bottom depths, and have maximum skill when the bottom depth lies at ~50-150m, depending upon latitude. For the southern sub-region at the shallowest depth bin, hindcast skill decreases rapidly with increasing lead time (Fig. 5a). However, as the bottom depth increases to ~100m, skill extends to longer lead times, still exceeding ~0.6 at 7-month lead. Below 100m, skill again decreases more rapidly with lead time, an effect that intensifies with increasing depth. Similar results are seen for the other sub-regions (Fig. 5b-c), although the northern sub-region is generally most skillful for leads greater than about 6 months, and more skillful than the central sub-region across almost all bottom depths.

By comparing hindcast skill to the forecast signal-to-noise ratios (section 2.3; Fig. 5d-f), we find that the local variations in hindcast skill (Fig. 5a-c) reflect variations in regional and depth-dependent predictability, rather than occurring by chance. In all three sub-regions, the signal-to-noise ratio first increases with increasing bathymetry depth, and then gradually decreases, tracking the depth dependence of BTA forecast skill at all latitudes (cf. Fig. 5d-f with Fig. 5a-c). In the southern sub-region, the depth dependence of the signal-to-noise ratio and total variance (cf. Fig. 5d with Fig. 6) are generally similar, whereas, for the other two sub-regions, BTA variance decreases monotonically with increasing bottom depth (Fig. 6). This contrast highlights the relatively higher predictability for bottom depths of ~50-150m, and for the northern sub-region. That is, in the northern sub-region, although the BTA variance and its predictable portion are both small, the noise is smaller, resulting in a relatively large signal-to-noise ratio and prediction skill extending to longer lead times.

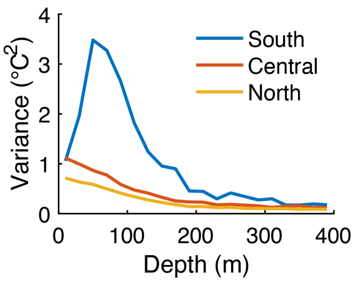

Figure 6. BTA variance as a function of bathymetry depth, separately evaluated for southern (blue), central (red), and northern (yellow) sub-regions.

3.4 Optimal BTA Evolution linked to ENSO

To help diagnose the dynamics contributing to BTA prediction skill, we identify the 7-month-lead “optimal precursor”, the initial conditions of coastal BTA, Pacific SSTA and SSHA that will most efficiently develop into large amplitude BTA after 7 months (Section 2.3). We then identify a subset (top 20%) of the observed states that most strongly resemble (i.e., project onto) this optimal precursor, and compare their subsequent observed composite evolution to that predicted by the LIM. This also helps identify potential forecasts of opportunity (Section 2.3). The top 20% selected states consist of top 10% warm and top 10% cold samples. Cold samples are multiplied by -1 prior to deriving the composite.

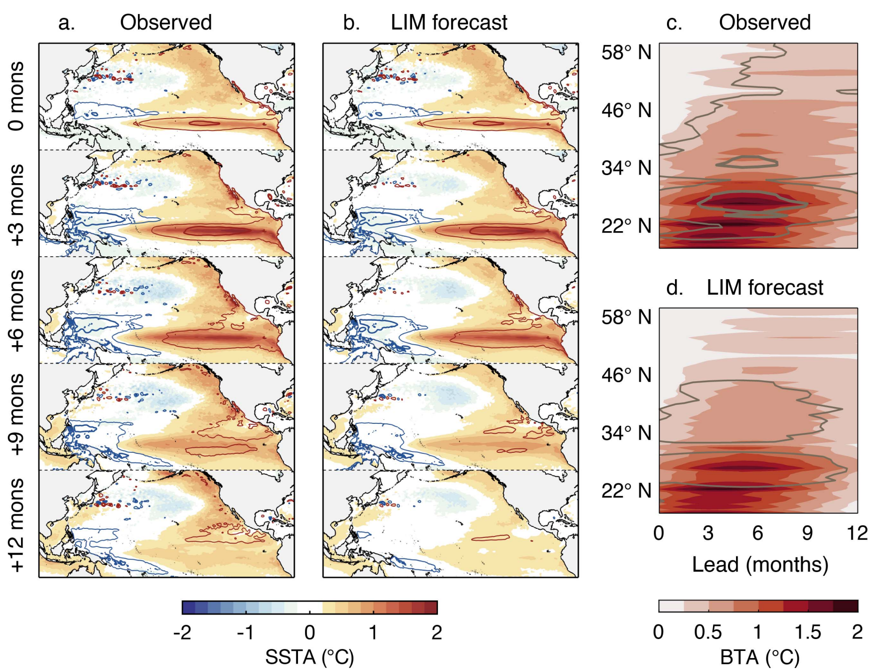

Figure 7. Forecast of opportunity identified by the optimal growth approach, and compared to observations (i.e., GLORYS12v1 reanalysis). (a-b) Lead 0 month plots the composite of the top 20% initial conditions that are most similar to the LIM's optimal precursor for coastal BTA. (a-b) Subsequent evolution at lead 3, 6, 9, 12 months is also composited, for (a) observations, and (b) LIM forecasts that are initialized from that top 20% conditions. Shading is SSTA. Contour is SSHA at 0.05m (thin), 0.1m (thick) (positive: red; negative: blue). (c-d) The top 20% initial BTA (shading) at 0 month and subsequent evolution at lead 1-24 month is composited, for (c) observation and (d) LIM forecast. Lead time is on x-axis. Latitude is on y-axis. The coastal SSTA is shown with contours at 0.6ºC (thin), 1.2ºC (thick).

The SSTA component of the observed initial condition for the resulting warm-minus-cold composite (shading of Fig. 7a at 0-month lead) features warm anomalies in the central and eastern tropical Pacific and in the Northeast Pacific. Its observed composite evolution shows strengthened warm anomalies in the tropical Pacific at 3- and 6-month leads, with subsequent decay at 9- and 12-month leads. Meanwhile, the initial SSHA component (contours in Fig. 7a at 0-month lead) exhibits positive (negative) anomalies in the eastern (western) tropical Pacific. The east-west SSHA dipole structure in the tropical Pacific strengthens at 3- and 6-month leads, and then weakens at 9- and 12-month lead, consistent with ENSO development.

The composite evolution of the observed BTA shows northward progression of the ENSO influence, with intensified BTA amplitudes occurring at longer lead time for higher latitudes (shading in Fig. 7c). The observed BTA evolution is obtained by deriving the coastal spatial pattern for each lead time and taking a spatial average for each latitudinal bin (0.6º bin width, similar to the process of deriving Fig. 2d), and is shown in a Hovmöller diagram. At 0-month lead, warm BTA is shown along the coastal domain, with stronger anomalies in the south and weaker in the north. As lead time increases, warm anomalies in the southern sub-region are gradually intensified, reaching a peak magnitude at ~3-to-6-month lead, and then decay, whereas in the northern part of the domain the peak magnitude occurs at a later lead time. Meanwhile, the coastal SSTA evolution is in phase with BTA (cf. contour with shading of Fig. 7c). Together with the Pacific evolution shown in Fig. 7a, these results suggest that the observed BTA amplification in the southern part of the domain coincides with ENSO development in the tropical Pacific, as both peak at the same lead time. For regions further away from the tropical Pacific, it takes a longer time for ENSO related influences to arrive and affect the local temperature variability, hence the delayed BTA amplification.

The result in Fig. 7 is not dominated by either warm or cold ENSO phase. To show this, we can separately analyze either the top 10% warm events (Fig. 8a) or the top 10% cold events (Fig. 8b). In both cases, although we have further reduced the sample sizes, we find similar results to those obtained from the warm-minus-cold composite: the analysis based on the top 10% warm (cold) conditions links the positive (negative) BTA growth and forecast skill to the development of El Niño (La Niña) in the tropical Pacific (not shown), with a northward progression of the ENSO influence.

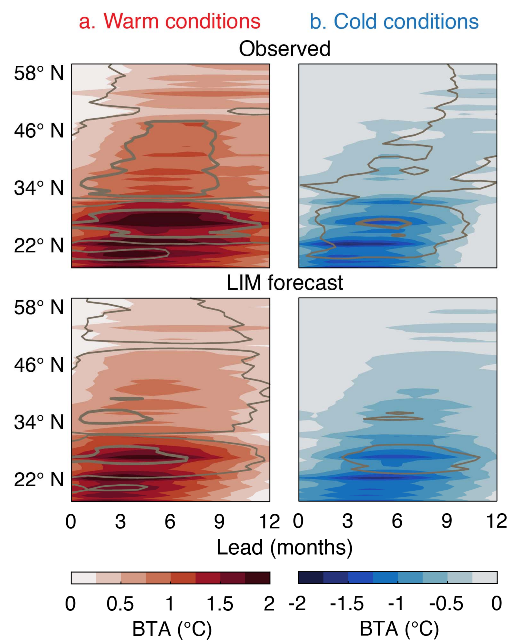

Figure 8. Same as Fig. 7c-d except for the top 10% (a) warm conditions, (b) cold conditions.

Lastly, Fig. 7b and 7d show that our LIM forecast, initialized with the optimal initial condition, largely captures the observed composite's anomaly growth and evolution, until reaching the longer lead times when the magnitude is somewhat underestimated. More importantly, forecasts whose initial conditions most resemble the optimal precursor have considerably elevated skill compared to the remaining forecasts (Fig. 9), suggesting that an initial high projection on the optimal precursor can identify a priori the most skillful BTA forecasts.

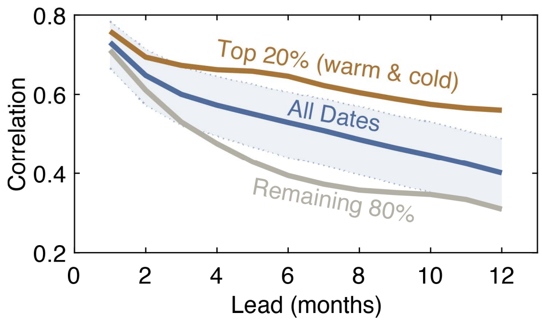

Figure 9. Skill of the hindcasts that are initialized from the top 20% initial conditions (brown), compared to skill of the remaining 80% hindcasts (gray), as well as hindcasts of all dates (blue). Skill is evaluated by spatially averaging the anomaly correlation within the coastal domain, for each lead. Blue shading represents the 95% confidence interval of the bootstrapped forecast skill.

4 Conclusions

In this study, using a LIM constructed from observed monthly Pacific SSTA, SSHA and coastal BTA, we investigated monthly BTA prediction along the North American West Coast for forecast leads of 1-to-12-months. The LIM's BTA hindcasts were considerably more skillful than persistence, with forecast skill (evaluated by anomaly correlation) exceeding 0.6 for much of the coastal region for lead times up to 6 months, and extending to even longer leads along the northernmost part of the coast. The season of maximum skill shifted from late fall to early spring from the southern to northern part of the coastal domain. Skill varies with bottom depth and is most pronounced at depths comparable to the depth of the thermocline along the North American West Coast, where variability can be large but the surface atmospheric noise is no longer felt.

The LIM allowed us to identify, a priori, forecasts with high prediction skill arising from initial conditions with a large projection on the optimal precursors of BTA growth. These forecasts of opportunity are characterized by anomaly evolution consistent with ENSO development, implying that ENSO is a major contributor to BTA prediction skill beyond persistence. The delay in the timing of the maximum skill from south to north is consistent with the ENSO influence on the North American West Coast occurring through different mechanisms that operate at different lags. The southern part of the domain, with small to no lags relative to ENSO development, can be expected to be more influenced by the northward propagation of coastally-trapped waves of equatorial origin, while at higher latitudes, where the BT hindcast skill lags ENSO peak phase by several months, the ENSO influence may be more likely associated with atmospheric teleconnections.

The individual processes associated with ENSO and their relative roles in BTA forecasts are not explicitly examined in this study. However, the skillful BTA hindcasts and their dependence on season, bottom depth and location, imply that the LIM is capable of implicitly incorporating these effects. Still, the explicit representation of these processes through the inclusion of additional variables, such as thermocline depth, ocean currents or surface winds, in the construction of the LIM, may further improve BT forecasts and shed light on the role of the individual mechanisms. This will require a follow-up study.

Acknowledgments

A.C. was supported by the NOAA Climate Program Office (CPO) and NOAA Climate Program Office Modeling, Analysis, Prediction and Projection (MAPP) Program.

Open Research

GLORYS12v1 reanalysis data are freely available at https://data.marine.copernicus.eu/product/GLOBAL_MULTIYEAR_PHY_001_030/services.

REFERENCES

Albers, J. R., and M. Newman, 2019: A priori identification of skillful extratropical subseasonal forecasts. *Geophys. Res. Lett.*, **46,** 12 527-512 536.

Alexander, M. A., L. Matrosova, C. Penland, J. D. Scott, and P. Chang, 2008: Forecasting Pacific SSTs: Linear inverse model predictions of the PDO. *Journal of Climate*, **21,** 385-402.

Alexander, M. A., I. Blade, M. Newman, J. R. Lanzante, N. C. Lau, and J. D. Scott, 2002: The atmospheric bridge: The influence of ENSO teleconnections on air-sea interaction over the global oceans. *Journal of Climate*, **15,** 2205-2231.

Alexander, M. A., J. D. Scott, M. G. Jacox, C. Deser, D. J. Amaya, A. Capotondi, and A. S. Phillips, 2023: A Survey of Coastal Conditions around the Continental US Using a High-Resolution Ocean Reanalysis. *Progress in Oceanography*, 103055.

Amaya, D. J., M. G. Jacox, J. Dias, M. A. Alexander, K. B. Karnauskas, J. D. Scott, and M. Gehne, 2022: Subseasonal-to-Seasonal Forecast Skill in the California Current System and Its Connection to Coastal Kelvin Waves. *Journal of Geophysical Research: Oceans*, **127,** e2021JC017892.

Amaya, D. J., M. G. Jacox, M. A. Alexander, J. D. Scott, C. Deser, A. Capotondi, and A. S. Phillips, 2023: Bottom marine heatwaves along the continental shelves of North America. *Nature Communications*, **14,** 1038.

Barbeaux, S. J., K. Holsman, and S. Zador, 2020: Marine heatwave stress test of ecosystem-based fisheries management in the Gulf of Alaska Pacific cod fishery. *Frontiers in Marine Science*, **7,** 703.

Breaker, L. C., 2019: Long-range persistence in sea surface temperature off the coast of central California. *Journal of Ocean and Climate*, **9,** 1759313118791113.

Breeden, M. L., B. T. Hoover, M. Newman, and D. J. Vimont, 2020: Optimal North Pacific Blocking Precursors and Their Deterministic Subseasonal Evolution during Boreal Winter. *Mon Weather Rev*, **148,** 739-761.

Breeden, M. L., J. R. Albers, A. H. Butler, and M. Newman, 2022: The Spring Minimum in Subseasonal 2-m Temperature Forecast Skill over North America. *Mon Weather Rev*, **150,** 2617-2628.

Capone, D. G., and D. A. Hutchins, 2013: Microbial biogeochemistry of coastal upwelling regimes in a changing ocean. *Nature Geoscience*, **6,** 711-717.

Capotondi, A., M. Newman, T. Xu, and E. Di Lorenzo, 2022: An Optimal Precursor of Northeast Pacific Marine Heatwaves and Central Pacific El Niño Events. *Geophysical Research Letters*, **49,** e2021GL097350.

Capotondi, A., P. D. Sardeshmukh, E. Di Lorenzo, A. C. Subramanian, and A. J. Miller, 2019a: Predictability of US West Coast Ocean Temperatures is not solely due to ENSO. *Scientific Reports*, **9,** 10.

Capotondi, A., C. Deser, A. S. Phillips, Y. Okumura, and S. M. Larson, 2020: ENSO and Pacific Decadal Variability in the Community Earth System Model Version 2. *J Adv Model Earth Sy*, **12,** e2019MS002022.

Capotondi, A., and Coauthors, 2019b: Observational Needs Supporting Marine Ecosystems Modeling and Forecasting: From the Global Ocean to Regional and Coastal Systems. *Frontiers in Marine Science*, **6**.

Chen, Z., and Coauthors, 2021: Seasonal Prediction of Bottom Temperature on the Northeast U.S. Continental Shelf. *Journal of Geophysical Research: Oceans*, **126,** e2021JC017187.

Deser, C., and M. L. Blackmon, 1995: On the Relationship between Tropical and North Pacific Sea Surface Temperature Variations. *Journal of Climate*, **8,** 1677-1680.

Ding, H., M. A. Alexander, and M. G. Jacox, 2021: Role of Geostrophic Currents in Future Changes of Coastal Upwelling in the California Current System. *Geophysical Research Letters*, **48,** e2020GL090768.

Drinkwater, K. F., and Coauthors, 2010: On the processes linking climate to ecosystem changes. *J Marine Syst*, **79,** 374-388.

Engida, Z., A. Monahan, D. Ianson, and R. E. Thomson, 2016: Remote forcing of subsurface currents and temperatures near the northern limit of the California Current System. *Journal of Geophysical Research: Oceans*, **121,** 7244-7262.

Farrell, B., 1988: Optimal excitation of neutral Rossby waves. *Journal of Atmospheric Sciences*, **45,** 163-172.

Frankignoul, C., G. Gastineau, and Y. O. Kwon, 2017: Estimation of the SST Response to Anthropogenic and External Forcing and Its Impact on the Atlantic Multidecadal Oscillation and the Pacific Decadal Oscillation. *Journal of Climate*, **30,** 9871-9895.

Frischknecht, M., M. Munnich, and N. Gruber, 2015: Remote versus local influence of ENSO on the California Current System. *Journal of Geophysical Research-Oceans*, **120,** 1353-1374.

Gómez-Valdivia, F., A. Parés-Sierra, and A. Laura Flores-Morales, 2017: Semiannual variability of the California Undercurrent along the Southern California Current System: A tropical generated phenomenon. *Journal of Geophysical Research: Oceans*, **122,** 1574-1589.

Hermann, A. J., E. N. Curchitser, D. B. Haidvogel, and E. L. Dobbins, 2009: A comparison of remote vs. local influence of El Niño on the coastal circulation of the northeast Pacific. *Deep Sea Research Part II: Topical Studies in Oceanography*, **56,** 2427-2443.

Hervieux, G., M. A. Alexander, C. A. Stock, M. G. Jacox, K. Pegion, E. Becker, F. Castruccio, and D. Tommasi, 2019: More reliable coastal SST forecasts from the North American multimodel ensemble. *Climate Dynamics*, **53,** 7153-7168.

Jacox, M. G., J. Fiechter, A. M. Moore, and C. A. Edwards, 2015: ENSO and the California Current coastal upwelling response. *Journal of Geophysical Research: Oceans*, **120,** 1691-1702.

Jacox, M. G., M. A. Alexander, C. A. Stock, and G. Hervieux, 2019: On the skill of seasonal sea surface temperature forecasts in the California Current System and its connection to ENSO variability. *Climate Dynamics*, **53,** 7519-7533.

Jacox, M. G., and Coauthors, in review: Downscaled seasonal forecasts for the California Current System: Skill assessment and prospects for living marine resource applications.

Jacox, M. G., and Coauthors, 2020: Seasonal-to-interannual prediction of North American coastal marine ecosystems: Forecast methods, mechanisms of predictability, and priority developments. *Progress in Oceanography*, **183**.

Kearney, K. A., M. Alexander, K. Aydin, W. Cheng, A. J. Hermann, G. Hervieux, and I. Ortiz, 2021: Seasonal Predictability of Sea Ice and Bottom Temperature Across the Eastern Bering Sea Shelf. *Journal of Geophysical Research: Oceans*, **126,** e2021JC017545.

Keller, A. A., L. Ciannelli, W. W. Wakefield, V. Simon, J. A. Barth, and S. D. Pierce, 2015: Occurrence of demersal fishes in relation to near-bottom oxygen levels within the California Current large marine ecosystem. *Fisheries Oceanography*, **24,** 162-176.

Kurczyn, J. A., P. Pérez-Brunius, M. López, J. Candela, F. Delgadillo-Hinojosa, and E. García-Mendoza, 2019: Water Masses and Ocean Currents Over the Continental Slope off Northern Baja California. *Journal of Geophysical Research: Oceans*, **124,** 2803-2823.

Lellouche, J., and Coauthors, 2021: The Copernicus Global 1/12 Oceanic and Sea Ice GLORYS12 Reanalysis, Frontiers in Earth Science, 9.

Liu, Z. Y., and M. Alexander, 2007: Atmospheric bridge, oceanic tunnel, and global climatic teleconnections. *Reviews of Geophysics*, **45**.

Lorenz, E. N., 1963: Deterministic Nonperiodic Flow. *Journal of Atmospheric Sciences*, **20,** 130-141.

Lou, J. L., T. J. O'Kane, and N. J. Holbrook, 2020: A Linear Inverse Model of Tropical and South Pacific Seasonal Predictability. *Journal of Climate*, **33,** 4537-4554.

Mariotti, A., and Coauthors, 2020: Windows of Opportunity for Skillful Forecasts Subseasonal to Seasonal and Beyond. *Bulletin of the American Meteorological Society*, **101,** E608-E625.

Meinen, C. S., and M. J. McPhaden, 2000: Observations of Warm Water Volume Changes in the Equatorial Pacific and Their Relationship to El Niño and La Niña. *Journal of Climate*, **13,** 3551-3559.

Newman, M., and P. D. Sardeshmukh, 2017: Are we near the predictability limit of tropical Indo-Pacific sea surface temperatures? *Geophysical Research Letters*, **44,** 8520-8529.

Newman, M., P. D. Sardeshmukh, C. R. Winkler, and J. S. Whitaker, 2003: A Study of Subseasonal Predictability. *Mon Weather Rev*, **131,** 1715-1732.

Norton, E. L., and Coauthors, 2020: The Importance of Environmental Exposure History in Forecasting Dungeness Crab Megalopae Occurrence Using J-SCOPE, a High-Resolution Model for the US Pacific Northwest. *Frontiers in Marine Science*, **7**.

Ottersen, G., S. Kim, G. Huse, J. J. Polovina, and N. C. Stenseth, 2010: Major pathways by which climate may force marine fish populations. *J Marine Syst*, **79,** 343-360.

Penland, C., and P. D. Sardeshmukh, 1995: The Optimal-Growth of Tropical Sea-Surface Temperature Anomalies. *Journal of Climate*, **8,** 1999-2024.

Qiu, B., S. M. Chen, N. Schneider, and B. Taguchi, 2014: A Coupled Decadal Prediction of the Dynamic State of the Kuroshio Extension System. *Journal of Climate*, **27,** 1751-1764.

Ray, S., S. A. Siedlecki, M. A. Alexander, N. A. Bond, and A. J. Hermann, 2020: Drivers of Subsurface Temperature Variability in the Northern California Current. *Journal of Geophysical Research: Oceans*, **125,** e2020JC016227.

Sampaio, E., and R. Rosa, 2020: Climate change, multiple stressors, and responses of marine biota. *Climate Action***,** 264-275.

Sardeshmukh, P. D., G. P. Compo, and C. Penland, 2000: Changes of Probability Associated with El Niño. *Journal of Climate*, **13,** 4268-4286.

Scaife, A. A., and D. Smith, 2018: A signal-to-noise paradox in climate science. *npj Climate and Atmospheric Science*, **1,** 28.

Shin, S. I., and M. Newman, 2021: Seasonal Predictability of Global and North American Coastal Sea Surface Temperature and Height Anomalies. *Geophysical Research Letters*, **48**.

Siedlecki, S. A., and Coauthors, 2016: Experiments with Seasonal Forecasts of ocean conditions for the Northern region of the California Current upwelling system. *Scientific Reports*, **6**.

Stock, C. A., and Coauthors, 2015: Seasonal sea surface temperature anomaly prediction for coastal ecosystems. *Progress in Oceanography*, **137,** 219-236.

Stock, C. A., and Coauthors, 2011: On the use of IPCC-class models to assess the impact of climate on Living Marine Resources. *Progress in Oceanography*, **88,** 1-27.

Wen, C., Y. Xue, and A. Kumar, 2012: Seasonal Prediction of North Pacific SSTs and PDO in the NCEP CFS Hindcasts. *Journal of Climate*, **25,** 5689-5710.

Xu, T., M. Newman, A. Capotondi, and E. Di Lorenzo, 2021: The Continuum of Northeast Pacific Marine Heatwaves and Their Relationship to the Tropical Pacific. *Geophysical Research Letters*, **48,** 2020GL090661.

Xu, T., M. Newman, A. Capotondi, S. Stevenson, E. Di Lorenzo, and M. A. Alexander, 2022: An increase in marine heatwaves without significant changes in surface ocean temperature variability. *Nature Communications*, **13,** 7396.

Zhao, Y., M. Newman, A. Capotondi, E. Di Lorenzo, and D. Sun, 2021: Removing the Effects of Tropical Dynamics from North Pacific Climate Variability. *Journal of Climate*, 1-49.